Maikel Rheinstädter*, Laura Toppozini, and Hannah Dies

The Interaction of Bio-Molecules with Lipid Membranes Studied by X-ray Diffraction

Abstract: For the past 100 years, X-ray diffraction has been a powerful and indispensable tool to study the structure of matter. The challenge when studying molecular ordering in biological materials is their inherent disorder and strong fluctuations, which often suppress the formation of Bragg peaks. In the case of membranes, X-rays can detect molecules inside and confined between membranes. In this article we review examples to highlight the capabilities and accomplishments of X-ray scattering for the determination of membrane structure. X-ray diffraction gives quantitative information about partitioning of a small molecule, ethanol, in lipid bilayers. By taking amyloid-β peptides as examples, it is demonstrated that the position of peptides in lipid membranes can be determined with high precision. Confinement between membranes can organize molecules, as is the case for a mono-nucleotide, adenosine monophosphate, and the resulting pattern might be important to understand the formation of short RNA strands. With new approaches and techniques, and the increasingly powerful and capable devices, X-ray diffraction will continue to be the work horse for the determination of molecular structure in biological materials.

Keywords: Lipid Membranes, X-ray Diffraction, Ethanol, Amyloid-β_{25-35} Peptide, Amyloid-β_{1-42} Peptide, Adenosine Monophosphate (AMP), Electron Density, Molecular Structure.

DOI 10.1515/zpch-2014-0541
Received May 30, 2014; accepted July 8, 2014

***Corresponding Author: Maikel Rheinstädter,** Department of Physics and Astronomy, McMaster University, 1280 Main Street West, Hamilon ON, L8S 3Z5, Canada, e-mail: rheinstadter@mcmaster.ca
Laura Toppozini, Hannah Dies: Department of Physics and Astronomy, McMaster University, 1280 Main Street West, Hamilon ON, L8S 3Z5, Canada

1 Introduction

The ongoing success of X-ray scattering to determine molecular and atomic structure is celebrated in 2014 by the 100 Years of X-ray Crystallography. Starting with the seminal work by the Braggs, 28 Nobel Prizes related to structure by X-ray (and neutron) scattering were awarded. X-ray crystallography is most useful and provides the highest resolution structures when the molecules are organized in a regular, crystalline environment. However, biological materials, in particular under physiological conditions, are inherently disordered and highly dynamic in nature. Fluctuations of different coherence lengths may lead to the formation of static or dynamic patches, so-called rafts [1–7]. The challenge that we are facing today is to get the most amount of structural information out of this disordered, dynamic state of matter.

Membranes are the most important biological interface. Their interaction with molecules plays a key role in the pathology of many diseases [8]. The determination of molecular structure and dynamics of biological membranes is one of the greatest challenges in modern biophysics. Few experimental techniques can access structural and dynamical properties on the nanometer scale and resolve dynamics of lipids, membrane-active molecules, and proteins and peptides [9–15]. Advanced X-ray and neutron scattering techniques have proven to be powerful tools to study structure, dynamics and interactions in synthetic and biological membranes down to nanometer length scales and nanosecond time scales.

Modern research also addresses more fundamental aspects of the interactions between X-rays, neutrons and biological materials in order to develop new ways to determine structure in semi-disordered and fluctuating materials. These materials are at the interface between crystals with infinite order and completely disordered materials with solely nearest neighbor correlations, which has a distinct effect on the pattern of Bragg peaks and extinction rules [16–18].

In this article we review examples to highlight the capabilities of X-ray diffraction in determining the molecular structure of lipid membranes, the interaction of small molecules with lipid membranes and their location and organization in the bilayers. X-ray diffraction is capable of determining molecular structure and ordering with sub nanometer resolution. Because the X-rays used in these studies only weakly interact with the so-called CHNOPS (the six most abundant biological elements), they are capable of penetrating the bilayers and detecting molecules inside membranes, as well as molecules confined between bilayers. In the first example in Section 2, the partitioning of ethanol in lipid membranes was determined from measuring electron density profiles. X-ray diffraction was used to determine the position of the molecule in the membranes and, in particular, determining

quantitative partitioning coefficients. High resolution X-ray diffraction can also be used to determine the precise location of peptides in lipid bilayers. Comparison between the experimentally determined electron profile with electron density calculations provides unprecedented resolution, as demonstrated by determining the position of amyloid-β peptides in anionic lipid membranes in Section 3. While hydrophilic molecules may not partition in the hydrocarbon membrane core, they may still interact with the lipid bilayer. The third example (Section 4) shows that adenosine monophosphate nucleotides form ordered arrays when confined between stacked bilayers, and demonstrates how X-ray diffraction can be used to study ordering of these molecules.

2 Partitioning of ethanol in lipid membranes

When partitioning into the bilayer, ethanol has been found to reside predominately at the membrane/water interface [19, 20]. The ethanol molecules can form hydrogen bonds with the lipid head groups with bond lifetimes of about 1 nanosecond [20, 21]. Ethanol has numerous effects on the lipid bilayer: it decreases the gel-to-fluid transition temperature [22, 23], it has a weak effect on the area per lipid, and it increases membrane fluidity and disorder [20]. Finally, and perhaps most importantly, ethanol has been found to increase membrane permeability [20, 24, 25]. Experiments using X-ray or neutron scattering to probe molecular dynamics and structure are scarce [26–29], most likely due to experimental challenges.

Toppozini et al. have recently demonstrated [29] that X-ray diffraction can provide quantitative information about the partitioning of small molecules in membranes. Due to the volatility of ethanol, it is necessary that the bilayers are in direct contact with a water/ethanol solution to ensure a well defined ethanol concentration in the membranes. For this reason, highly concentrated suspensions of 1,2-dimyristoyl-sn-glycero-3-phoshatidylcholine (DMPC) were prepared by hydrating the lipid powder using a 5 wt % ethanol solution, as shown in Figure 1a. This concentration is significantly larger than alcohol concentrations of ~0.092 wt % (~0.036 mol %) found in human blood [30]. However, 5 wt % can be considered a moderate alcohol concentration to which skin and mucous membranes in mouth and digestive system can be exposed.

X-ray scans were measured for pure DMPC bilayers and DMPC/ethanol at two temperatures, namely $T = 293$ K, in the gel phase for DMPC bilayers, and $T = 303$ K, in their fluid phase, as shown in Figure 1b). The pronounced Bragg

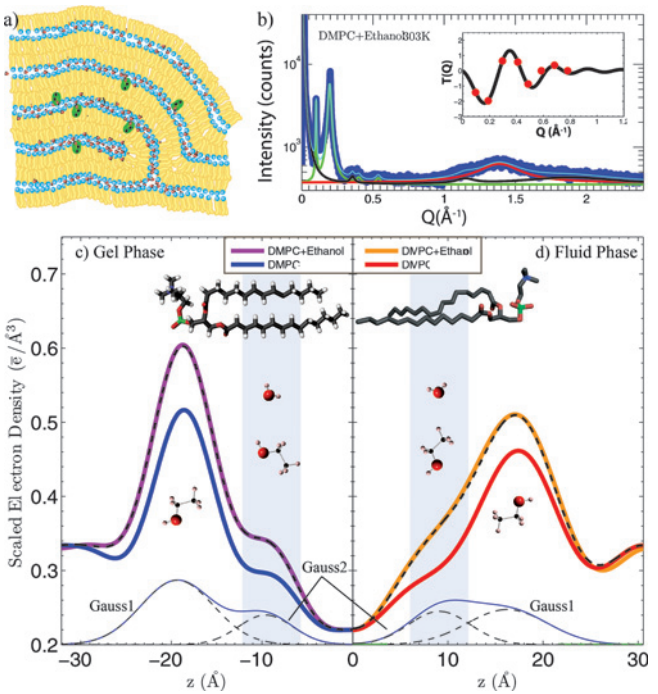

Figure 1: a) Schematic of the lipid powder hydrated with H_2O and ethanol. Non-oriented bilayers are formed. b) As the randomly oriented membranes act as a powder sample, lamellar and in-plane Bragg peaks are observed in the same scan, however on different length scales. Q is the total scattering vector defined by $Q = 4\pi \sin(\theta)/\lambda$. Phases were selected based on the $T(q_z)$ function (inset). c) Electron density for the DMPC and DMPC/ethanol membranes in their gel phase. d) Electron density for the membranes in the fluid phase. An increase in electron density in the samples with ethanol in both c) and d) points to ethanol molecules residing in the head group region and ethanol and/or water amongst the hydrophobic tails. Figure adapted from [29].

peaks at Q values up to ~ 0.75 Å^{-1} are the result of a multi-lamellar membrane structure in the powder.

The additional correlation peaks at higher Q values are caused by the in-plane structure of the membranes. The lipid tails form a densely packed structure with hexagonal symmetry (planar group p6) [3] and the distance between two acyl tails is calculated to be $a_T = 4\pi/(\sqrt{3}q_T)$. The corresponding correlation peaks were observed at $q_T \sim 1.49$ Å^{-1} in both the DMPC and DMPC/ethanol systems at $T = 293$ K, corresponding to a distance between neighbouring acyl chains of ~ 4.87 Å in the gel phase. In the fluid phase, the lipid tail positional correlation peaks occur at

1.39 $Å^{-1}$ in the DMPC and DMPC/ethanol samples at $T = 303$ K, corresponding to an increased distance between neighbouring acyl chains of ~ 5.22 Å.

The lamellar Bragg peaks were fit using Lorentzian peak profiles. Up to eight peaks could be fit and were used to reconstruct the electron density. The inset to Figure 1b) shows the bilayer form factor, $T(q_z)$, for DMPC in its gel phase as example, which was used to assess the corresponding array of phases out of the 2^8 combinations, assuming a phase of +1 or −1.

The integrated intensities of the lamellar Bragg peaks were used in a Fourier transform to calculate the electron density profiles perpendicular to the bilayers, as shown in Figure 1c and d. In order to put $\rho(z)$ on an absolute scale, the electron densities were scaled to fulfil the condition $\rho(0) = 0.22\ e/Å^3$ (the electron density of a CH_3 group at the end of a lipid tail) in the centre of the bilayer, and $\rho(d_z/2) = 0.330\ e/Å^3$, the electron density for water/5 wt % ethanol outside the bilayers. The normalized electron density profiles for DMPC and DMPC/ethanol in gel phase are shown in Figure 1c). The profile corresponds to a DMPC molecule in the well ordered gel state with both chains in all-trans configuration [31–33]. The electron rich phosphorous group in the head group region can be identified by the peak in the electron density at ~ 22 Å. $\rho(z)$ monotonically decreases towards the bilayer centre at $z = 0$; only CH_3 group at the end of the lipid tails are found in the centre.

The presence of ethanol leads to an increase in electron density in the head group region of the bilayers. $\rho(z)$ is also increased around z values of ~ 9 Å, indicating the presence of molecules that have permeated the membrane. The dip in the electron densities at z values of ~ 27 Å is most likely related to a reduced density of the hydration water and solvent at the lipid/solvent interface. The position of the ethanol molecules in the bilayers was determined under the assumption that small amounts of added molecules do not change the structure of the bilayers significantly, such that the change in electron density can be attributed to ethanol molecules. The addition of two Gaussian peak profiles ($\rho(z) = \rho_0 \exp[-(z - z_0)^2/2\sigma^2]$) to the electron density profiles of pure DMPC in Figure 1c and d results in the dashed black lines, which show excellent agreement to the DMPC/ethanol data. In the gel phase, Gauss 1 is centred at 19.35 Å and Gauss 2 is centred at 9.6 Å, whereas for the fluid phase we obtain the Gauss 1 centred at 16.25 Å and Gauss 2 centred at 9.1 Å.

The number of ethanol molecules in the head group region can be determined by further analysis of the areas of the Gaussian peaks. The number of electrons related to the electron density in the Gaussian peaks is calculated by $e^- = A_L \int_{\text{Gauss}} \rho(z)dz$. By dividing this number by the number of electrons of an ethanol or water molecule, the number of ethanol or equivalent water molecules per lipid molecule can be determined. As the X-ray experiment is averaging over

a large number of unit cells, a non-integer occupancy means that ethanol (or water) molecules can be shared between lipids. The increase in electron density corresponds to ~ 1.6 ethanol molecules per lipid molecule in the gel phase. The number of ethanol molecules assigned to Gaussian 1 in the fluid phase is slightly less, ~ 1.2 ethanol molecules per lipid molecule.

Gaussian 2 can not be unambiguously assigned to the presence of either ethanol or water molecules solely based on the electron density. If Gaussian 2 is related to the presence of additional ethanol molecules in the membrane core, the increase in electron density corresponds to 0.55 ethanol molecules per lipid molecule in the gel phase and 0.85 ethanol molecules per lipid molecule in the fluid phase. It is believed that general anaesthetics, such as ethanol, dissolve in membranes thereby changing their physical properties and altering membrane function [34]. Changes in lateral pressure are speculated to be relevant for protein function and binding sites, and in particular functioning of ion channels [35]. The potential presence of ethanol molecules in the hydrophobic core is likely to be important to distinguish between different theories [35–38]. The presence and solubility of ethanol molecules in the hydrophobic core might also be relevant to model ethanol crossing events [20, 39, 40].

When Gaussian 2 is assigned to the presence of water molecules in the hydrophobic membrane core, the increase in electron density corresponds to 1.42 water molecules per lipid molecule in the gel state of the phospholipid membranes. In the fluid phase at $T = 303$ K (Figure 1 d), 2.22 water molecules per lipid molecule is dissolved in the hydrophobic membrane core.

Measuring membrane/ethanol and membrane/water partition coefficients in the presence of ethanol has proven to be difficult due to experimental challenges, mainly related to the small volumes and the volatility of the ethanol molecule. Partition coefficients must be measured in-situ, directly on lipid bilayers [30, 40–45]. X-ray diffraction can quantitatively determine partition coefficients of small molecules in membranes in their physiologically relevant fluid phase. While the presence of water in the hydrophobic membrane core is indicative of an increased permeability, additional ethanol molecules in the core emphasize ethanol's function as an anesthetic. However, water and ethanol molecules cannot easily be distinguished in X-ray experiments. This is the domain of neutron diffraction using membranes with deuterium labeled ethanol or water molecules.

3 Position of amyloid-β peptides in lipid membranes

The interactions of proteins with lipid membranes play a large role in maintaining the integrity and functionality of the cell membrane, and significant changes in these interactions are involved in the pathology of many diseases [8]. Misfolding and aggregation of Aβ peptides, specifically, is involved in the development of Alzheimer's disease, although the exact relationship between the protein structure and the pathology of Alzheimer's is still unclear [46]. Aβ consists of a polypeptide with 42 amino acids, 10 of which (segment 25-35) comprise the transmembrane segment of the amyloid precursor protein (APP) and also comprise part of the full length Aβ peptide. As such, this short transmembrane segment is often used in studies of the protein interactions and partitioning in the membrane [47, 48].

While Aβ peptides are frequently reported in an extracellular location, Aβ_{1-40} and Aβ_{1-42} molecules were found to strongly interact with negatively charged lipids and to bind to anionic, negatively charged membranes [49–55], orienting parallel to the membrane surface. Through X-ray and neutron diffraction, Mason et al. [56] and Dante, Hauß and Dencher [47] observed an embedded state for the Aβ_{25-35} segment and the full-length Aβ_{1-42} peptide in anionic lipid membranes [57].

X-ray diffraction is a prime tool to study the interaction between amyloid peptides and lipid membranes, and their location in the bilayers. The preparation of highly oriented, multi lamellar membranes offers (1) a good signal by using several thousands of stacked membranes and (2) the advantage that the lateral (in-plane) and transverse (out-of-plane) membrane structure can be studied separately, however simultaneously. Atomic resolution protein structures are routinely determined by protein X-ray-crystallography from protein crystals. This approach fails when proteins are embedded in membranes as the resulting structure is inherently disordered. The absence of higher order Bragg reflections prevents an atomic resolution structure determination. However, when high resolution electron densities are compared with electron densities calculated for protein structures determined by protein crystallography or NMR, the location of the peptide in the bilayer can be determined with sub-nanometer resolution.

In a recent study by Dies et al. [58], anionic lipid membranes were prepared with 97 mol % 1,2-dimyristol-sn-glycero-3-phosphatidylcholine (DMPC), a 14 chain saturated phospholipid with an overall zwitterionic nature, and 3 mol % 1,2-dimyristol-sn-glycero-3-phospho-L-serine (DMPS), a 14 chain saturated anionic phospholipid, as sketched in Figure 2a. Figure 2b shows a sketch of

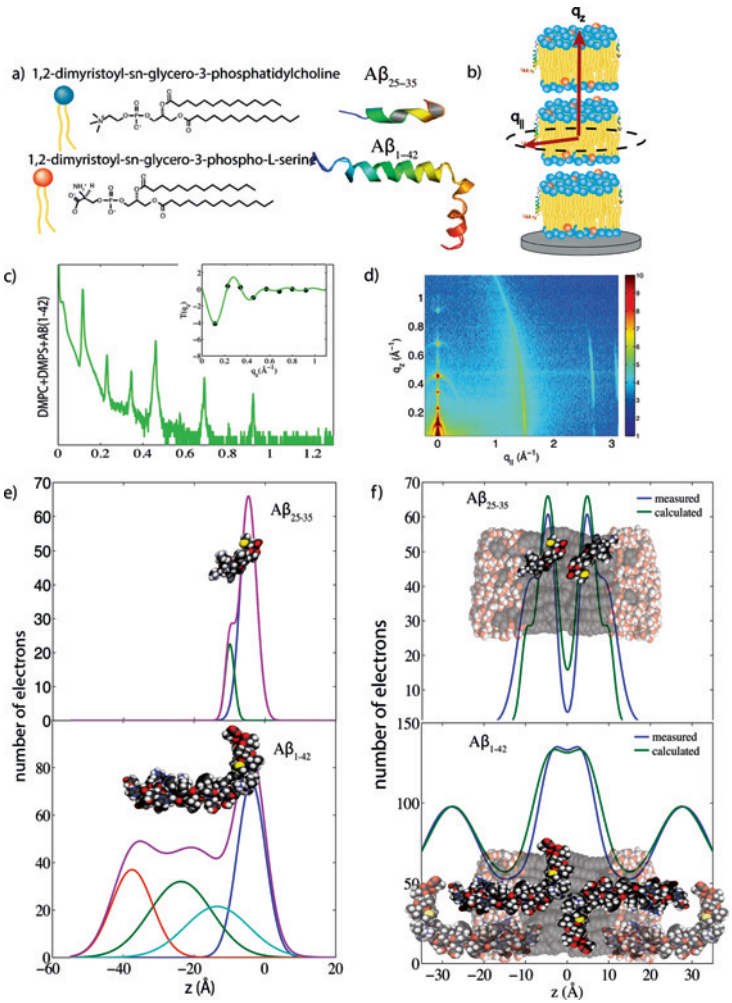

Figure 2: a) Schematic representations of DMPC, DMPS, amyloid-β_{25-35} and amyloid-β_{1-42} molecules. b) Diagram of the solid supported, multi-lamellar membranes used for the X-ray diffraction measurements. Two-dimensional data sets were collected to study molecular structure perpendicular to the solid supported membranes (out-of-plane, q_z) and parallel to the membranes (in-plane, $q_{||}$). c) Reflectivity measurement for samples containing 3 mol % Aβ_{25-35}. Fourier transforms of the reflectivity data using the shown phases (inset) provides the electron density perpendicular to the membrane. d) 2-dimensional X-ray diffraction measurements for a membrane sample containing 3 mol % Aβ_{1-42}. e) Electron distribution for the Aβ_{25-35} (top) and Aβ_{1-42} (bottom) peptides obtained from modelling of PDB structural information. f) Comparison between electronic structure predictions obtained from analysis of PDB structural information and the measured distributions obtained from X-ray reflectivity measurements, for both the Aβ_{25-35} (top), and the Aβ_{1-42} (bottom) peptides. Adapted from [58]

the solid supported membrane stacks prepared. While fully hydrated liquid crystalline samples are generally assumed to best mimic physiologically relevant conditions, these disordered bilayers do not diffract well, i.e. they give rise to a limited number of Bragg peaks, and as such do not lend themselves ideally to traditional crystallographic analysis. As high resolution structural data are needed, which involves the collection of high order Bragg peaks, these studies were conducted in a dehydrated state of the membranes [59]. This situation is similar to protein crystallography, where protein crystals are investigated at liquid nitrogen temperatures. While it is generally assumed that peptide positions and conformations are preserved under physiological conditions, the experimental findings are strictly valid only under the conditions data were obtained.

A large map of the reciprocal space is shown in Figure 2d and indicates that homogeneous and well oriented and defect-free membranes form for this system. A reflectivity scan of a DMPC/DMPS membrane containing 3 mol % Aβ_{1-42} is depicted in Figure 2c and shows a series of pronounced and equally spaced lamellar Bragg peaks due to the multi-lamellar structure of the membranes [10, 11]. The corresponding phases were assessed from the corresponding bilayer form factor in the inset. The electron densities were then determined from the integrated peak intensities of the lamellar peaks.

In order to obtain absolute electron densities, ρ_z for the pure lipid DMPC/DMPS bilayers was scaled to fulfil the condition $\rho(0) = 0.22\ \mathrm{e/\AA^3}$ (the electron density of a CH_3 group) in the center of the bilayer. The electron density between two stacked bilayers, $\rho(d_z/2)$, is often scaled to the electron density of bulk water, which is a good approximation in single component model membranes. The addition of DMPS to the DMPC bilayers, a phospholipid whose net +1 charge may result in a nonuniform distribution of head groups at the head group-water interface. In addition, membrane embedded or surface bound peptides are likely to change the structure at the water/bilayer interface. The electron densities were, therefore, scaled such that the integral of the electron density across the bilayer, multiplied by the area per lipid yielded the required number of electrons.

The average electron density of an amino acid is calculated to be $\rho(0) = 0.33\ \mathrm{e/\AA^3}$. The electron densities at the bilayer center, $\rho(0)$, for the peptide samples were scaled to values $0.22\ \mathrm{e/\AA^3} < \rho(0) < 0.33\ \mathrm{e/\AA^3}$ until a good agreement with the peptide structure calculations was achieved. Best agreement for the Aβ_{1-42} peptide in Figure 2f was obtained for a value of $\rho(0) = 0.33\ \mathrm{e/\AA^3}$, indicative that mainly amino acids reside in the bilayer center, in agreement with the proposed position. A value of $\rho(0) = 0.22\ \mathrm{e/\AA^3}$ provided good agreement between experiment and calculation for the Aβ_{25-35} fragment, indicating that this peptide does not take a trans-membrane position.

The in-solution structures of the Aβ_{25-35} fragment (sequence ^{25}G-S-N-K-G-A-I-I-G-L-^{35}M) and the full length Aβ_{1-42} peptide were reported by D'Ursi et al. [60] and Crescenzi et al. [61] from nuclear magnetic resonance (NMR). The corresponding structure files are deposited in the Protein Database (PDB) as 1QWP (Aβ_{25-35}) and 1IYT (Aβ_{1-42}). X-ray diffraction is sensitive to the electronic structure of bilayers and peptides. In order to compare the experimentally determined electronic profiles, the PDB structures were used to calculate 1-dimensional projections of the electron distributions along the long z-axis of the peptides. To take into account thermal motions of atoms and electrons, each atom was modeled by a Gaussian distribution with a width (FWHM) of 4 Å, and the corresponding electron distributions were summed. The results are plotted in Figure 2e. In both peptides, the methionine at position 35 is discernable because of its electron rich sulphur atom.

By subtracting the electron density of the anionic lipid matrix and the electron density in the presence of the peptides, the electronic distribution of the membrane-embedded peptides was obtained and compared to the calculation. Best agreement between calculation and experiment was obtained for the peptide location and orientation in Figure 2f. We note that this approach is strictly correct only under the assumption that the lipid matrix is not altered upon introduction of the peptide. Buchsteiner et al. [62] and Buchsteiner, Hauß and Dencher [63] have shown that the structure of the membranes is unaffected at a low peptide concentration of 3 mol %.

The exact locations of the peptides are prerequisites for understanding the interactions of the peptide with the membrane. They are of particular importance as the interaction between membrane-embedded peptides is a membrane-mediated elastic interaction with strong dependence on the membrane environment [12, 64, 65], rather than a direct peptide-peptide interaction. The interaction between peptides and membranes is often modelled by the two-stage or two state-model [66–68]. In a first step, the peptide makes contact with the membrane and aligns parallel to the membrane, before stronger bonds form and the peptide is embedded into the hydrocarbon core. The penetration of peptides into the membrane is believed to be a crucial step in oligomerization or fibrillation, and thus important to understand the pathology of amyloidogenic disease.

4 Adenosine monophosphate forms ordered arrays when confined between lipid bilayers

While the above examples demonstrate that X-ray diffraction is a prime tool to detect molecules inside membranes, lipid bilayers can also serve to confine and or-

ganize molecules. There is a consensus that a form of life based primarily on RNA likely preceded the RNA-DNA-protein world of the ancestral cell. However, in the absence of enzymes and metabolism there has been no obvious way for RNA-like molecules to be produced [69] and then encapsulated in cellular compartments, an essential first step in the origin of cellular life. Cycles of hydration and dehydration at elevated temperatures can be used to simulate conditions in the neighborhood of volcanic hydrothermal springs. Rajamani et al. [70] showed that such conditions activate condensation reactions that can polymerize mononucleotides organized in a lipid matrix.

Toppozini et al. recently investigated 5'-adenosine monophosphate (AMP) molecules captured in a multilamellar phospholipid matrix composed of 1,2-dimyristoyl-sn-glycero-3-phoshatidylcholine (DMPC) and observed Bragg peaks corresponding to the lateral organization of the confined AMP molecules [73]. Instead of forming a random array or its free-form crystal structure [71], the AMP molecules were found to be highly entangled, with the phosphate and ribose groups in close proximity. This structure may facilitate polymerization of the nucleotides into RNA-like polymers.

Membrane complexes with different molar ratios of AMP molecules were studied. By preparing highly oriented, solid-supported lipid bilayers, the in-plane ($q_{||}$) and out-of-plane (q_z) structure of the membranes could be determined simultaneously. The experimental setup is sketched in Figure 3a and the molecular structure resulting from this analysis is shown in Figure 3b.

Figure 3c shows a 2-dimensional X-ray intensity map for AMP : DMPC in a molar ratio of 3 : 1. The lamellar spacing, d_z, of the membrane AMP complexes was determined from the specular reflectivity. Up to 24 Bragg peaks could be identified for a given sample and assigned to different d_z-spacings and phases. To assign the peaks to different phases, Braggs law was re-written as $n = 2d_z/\lambda \sin(\theta)$. By plotting the order of the different Bragg reflections against the sine of the Bragg angles, n vs. $\sin(\theta(n))$, peaks which belong to the same d_z-spacing fall on a straight line through the origin, whose slope is proportional to d_z, as shown in Figure 3d. The increase in lamellar spacing in the presence of AMP molecules can be compared to the spacing of a pure DMPC bilayer, $d_z - d_z^{lipid} = m\Delta d$, where m is an integer number. The data points for all concentrations were well fit by an increment of Δd of $\Delta d = 2.67$ Å. This value is in agreement to the thickness of an interstitial single layer of AMP molecules and indicative that the quasi 2-dimensional AMP molecules take a flat position between the stacked bilayers.

The lateral arrangement of lipid and AMP lead to the occurrence of in-plane diffraction peaks, as shown in Figure 3 e). The corresponding unit cell is rectangular with lattice parameters $a = 6.25$ Å and $b = 4.8$ Å. This 2-dimensional structure of the confined AMP molecules is significantly different from the structure of crys-

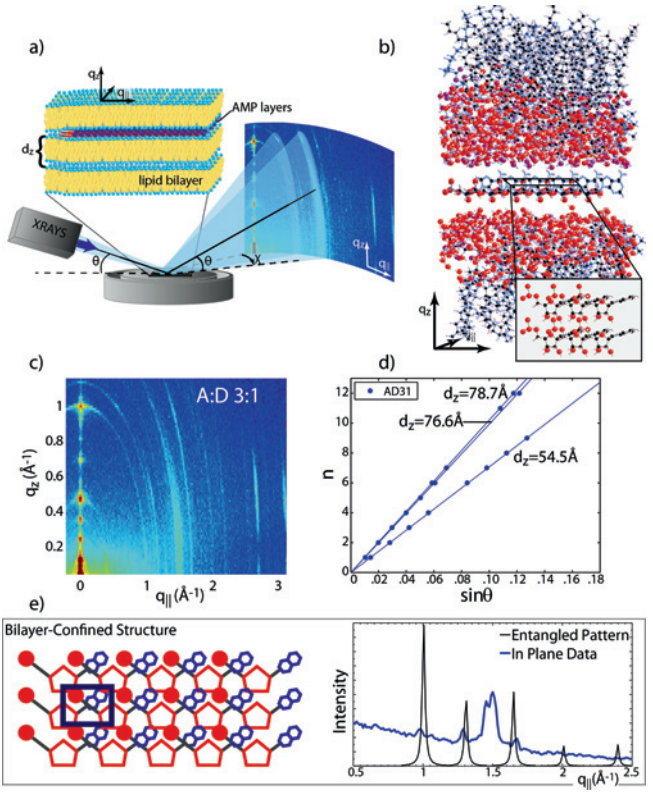

Figure 3: Schematic representations of the experimental setup, analysis and results AMP-DMPC confinement experiments [73]. a) Schematic of experimental X-ray setup. AMP molecules confined by lipid bilayers on BLADE sample stage from the Laboratory of Membrane and Protein Dynamics at McMaster University. An example 2D X-ray scan is shown. b) Molecular structure of one layer of AMP sandwiched between two lipid leaflets. c) 2D scan of a sample containing 3 parts AMP to 1 part lipid (molar) showing additional lamellar and in-plane reflections. d) Out-of-plane analysis of part c). Each line represents a d_z-spacing. Multiple d_z-spacings were observed in the presence of AMP between the bilayers. e) Schematic top-view of the confined AMP molecules. The plot shows the the agreement between theoretical (black) and experimental (blue) diffraction patterns. Figure adapted from [73].

talline AMP, which crystallizes in a less densely packed 3-dimensional monoclinic structure $P2_1$ with unit cell dimensions of $a = 12.77$ Å, $b = 11.82$ Å, $c = 4.882$ Å and $\beta = 92.24^\circ$ [72]. The corresponding molecular arrangement (see Figure 3 e)) brings the phosphate group of AMP in close proximity to the 3' position of the ribose. The distance between the two groups can be estimated from the molecular structure to be 2.1 Å. The observed pattern of the confined AMP molecules

may thus favor the formation of RNA-like polymers when the chemical potential provided by anhydrous conditions drives the synthesis of phosphodiester bonds between nucleoside monophosphates.

5 Conclusion

We highlighted three examples of how X-ray diffraction can provide quantitative information about the position and organization of small molecules in lipid bilayers. Because X-rays penetrate into the membranes, partition coefficients of small, volatile molecules in bilayers can be determined. This was demonstrated using ethanol as an example in Section 2 [29].

Protein crystallography provides atomic resolution protein and peptide structures. The missing crystal lattice prevents this approach for membrane embedded peptides. However, by comparing high resolution electron densities with atomic resolution peptide structures, position and orientation of peptides in lipid membranes can be determined with very high precision. The position of $A\beta_{1-42}$ and $A\beta_{25-35}$ peptides in anionic lipid membranes was determined using this approach in Section 3 [58].

Small molecules can also be confined between membranes. Layers of nucleotide molecules embedded between stacked membranes were observed when mixing mononucleotides with lipid molecules. The lipid matrix helped to organize the molecules into a pattern, which may facilitate fusion of the nucleotides into short RNA strands. High resolution X-ray diffraction is the perfect tool to detect ordering of these molecules and can give unprecedented information that cannot easily be obtained by other techniques [73].

These examples demonstrate the unique capabilities and importance of X-ray diffraction in systems, which are intrinsically disordered. With new approaches and techniques and the increasingly powerful and capable devices, X-ray diffraction will continue to be the work horse for the determination of molecular structure. Happy Birthday, X-ray diffraction.

Acknowledgement: This research was funded by the Natural Sciences and Engineering Research Council of Canada (NSERC), the National Research Council Canada (NRC), the Canada Foundation for Innovation (CFI) and the Ontario Ministry of Economic Development and Innovation. H. D. is the recipient of an NSERC Undergraduate Research Awards (USRA), L. T. is the recipient of an NSERC Canada Graduate Scholarship (CGS), M. C. R. is the recipient of an Early Researcher Award of the Province of Ontario.

References

1. K. Simons and E. Ikonen, Nature **387** (1997) 569.
2. K. Simons and M.J. Gerl, Nat. Rev. Mol. Cell. Bio. **11** (2010) 688.
3. C. L. Armstrong, D. Marquardt, H. Dies, N. Kučerka, Z. Yamani, et al., PLOS ONE **8** (2013) e66162.
4. S. Meinhardt, R. L. C. Vink, and F. Schmid, P. Natl. Acad. Sci. USA **110** (2013) 4476.
5. M. C. Rheinstädter and O. G. Mouritsen, Curr. Opin. Colloid In. **18** (2013) 440.
6. M. Barrett, S. Zheng, L. Toppozini, R. Alsop, H. Dies, et al., Soft Matter **9** (2013) 9342.
7. R. J. Alsop, M. A. Barrett, S. Zheng, H. Dies, and M. C. Rheinstädter, Soft Matter **24** (2014) 4275.
8. F. R. Maxfield and I. Tabas, Nature **438** (2005) 612.
9. T. Salditt and M. C. Rheinstädter, Structure and Dynamics of Model Membrane Systems Probed by Elastic and Inelastic Neutron Scattering, in: *Neutron Scattering in Biology, Techniques and Applications*, J. Fitter, T. Gutberlet, J. Katsaras (Eds.), Heidelberg: Springer (2006), pp. 503–-530.
10. G. Pabst, N. Kučerka, M. P. Nieh, M. Rheinstädter, and J. Katsaras, Chem. Phys. Lipids **163** (2010) 460.
11. G. Fragneto and M. Rheinstädter, C. R. Phys. **8** (2007) 865.
12. C. L. Armstrong, E. Sandqvist, and M. C. Rheinstädter, Protein Peptide Lett. **18** (2011) 344.
13. M. C. Rheinstädter, Lipid Membrane Dynamics, in: V. García Sakai, C. Alba-Simionesco, S. H. Chen (Eds.), *Dynamics of Soft Matter*, Neutron Scattering Applications and Techniques U. S. Springer, New York Dordrecht Heidelberg London (2012), pp. 263–286.
14. J. F. Nagle, Faraday Discuss. **161** (2013) 11.
15. M. C. Rheinstädter, Basic Aspects and Applications of Lipids and Protein Dynamics, in: *Liposomes, Lipid Bilayers and Model Membranes: from Basic Research to Application*, CRC Press, Boca Raton (2014), pp. 111–124.
16. S. Förster, A. Timmann, C. Schellbach, A. Frömsdorf, A. Kornowski, et al., Nat. Mater. **6** (2007) 888.
17. C. L. Armstrong, M. A. Barrett, L. Toppozini, N. Kučerka, Z. Yamani, et al., Soft Matter **8** (2012) 4687.
18. F. C. Yang, R. Peters, H. Dies, and M. C. Rheinstädter, Soft Matter **10** (2014) 5541.
19. P. Westerman, J. Pope, N. Phonphok, J. Doane, and D. Dubro, BBA-Biomembranes **939** (1988) 64.
20. M. Patra, E. Salonen, E. Terama, I. Vattulainen, R. Faller, et al., Biophys. J. **90** (2006) 1121.
21. B. W. Koenig and K. Gawrisch, J. Phys. Chem. B **109** (2005) 7540.
22. J. A. Barry and K. Gawrisch, Biochemistry **33** (1994) 8082.
23. S. E. Feller, C. A. Brown, D. T. Nizza, and K. Gawrisch, Biophys. J. **82** (2002) 1396.
24. H. Komatsu and S. Okada, Chem. Phys. Lipids **85** (1997) 67.
25. H. V. Ly and M. L. Longo, Biophys. J. **87** (2004) 1013.
26. T. Adachi, Chem. Phys. Lipids **107** (2000) 93.
27. M. D. Kaye, K. Schmalzl, V. C. Nibali, M. Tarek, and M. C. Rheinstädter, Phys. Rev. E **83** (2011) 050907.
28. H. Seto, M. Hishida, H. Nobutou, N. L. Yamada, M. Nagao, et al., J. Phys. Soc. Jpn. **76** (2007) 054602.

29. L. Toppozini, C. L. Armstrong, M. A. Barrett, S. Zheng, L. Luo, et al., Soft Matter **8** (2012) 11839.
30. D. T. Nizza and K. Gawrisch, Gen. Physiol. Biophys. **28** (2009) 140.
31. S. Nagle-Tristram, Y. Liu, J. Legleiter, and J. F. Nagle, Biophys. J. **83** (2002) 3324.
32. N. Kučerka, Y. Liu, N. Chu, H. I. Petrache, S. Tristram-Nagle, et al., Biophys. J. **88** (2005) 2626.
33. N. Kučerka, S. Tristram-Nagle, and J. F. Nagle, Biophys. J. **90** (2006) L83.
34. P. Seeman, Pharmacol. Rev. **24** (1972) 583.
35. H. Jerabek, G. Pabst, M. Rappolt, and T. Stockner, J. Am. Chem. Soc. **132** (2010) 7990.
36. K. Y. Y. Pang, L. M. Braswell, L. Chang, T. J. Sommer, and K. W. Miller, Mol. Pharmacol. **18** (1980) 84.
37. J. R. Trudell, Anesthesiology **46** (1977) 5.
38. D. Mountcastle, R. Biltonen, and M. Halsey, P. Natl. Acad. Sci. USA **75** (1978) 4906.
39. A. N. Dickey and R. Faller, Biophys. J. **92** (2007) 2366.
40. E. Terama, O. H. S. Ollila, E. Salonen, A. C. Rowat, C. Trandum, et al., J. Phys. Chem. B **112** (2008) 4131.
41. Y. Katz and J. Diamond, J. Membrane Biol. **17** (1974) 69.
42. Y. Katz and J. M. Diamond, J. Membrane Biol. **17** (1974) 101.
43. E. Rowe, Mol. Pharmacol. **22** (1982) 133.
44. C. Trandum, P. Westh, K. Jörgensen, and O. G. Mouritsen, Biochim. Biophys. Acta **1420** (1999) 179.
45. P. Westh and C. Trandum, Biochim. Biophys. Acta **1421** (1999) 261.
46. B. J. Gilbert, J. Clin. Pathol. **66** (2013) 362.
47. S. Dante, T. Hauss, and N. A. Dencher, Biophys. J. **83** (2002) 2610.
48. S. Dante, T. Hauß, and N. A. Dencher, Eur. Biophys. J. **35** (2006) 523.
49. M. del Mar Martínez-Senac, J. Villalaín, and J. C. Gómez-Fernández, Eur. J. Biochem. **265** (1999) 744.
50. E. Maltseva and G. Brezesinski, ChemPhysChem **5** (2004) 1185.
51. G. Thakur, M. Micic, and R. M. Leblanc, Colloid. Surface. B **74** (2009) 436.
52. M. A. Sani, J. D. Gehman, and F. Separovic, FEBS Lett. **585** (2011) 749.
53. F. Hane, E. Drolle, R. Gaikwad, E. Faught, and Z. Leonenko, J. Alzheimers Dis. **26** (2011) 485.
54. H. Ding, J. A. Schauerte, D. G. Steel, and A. Gafni, Biophys. J. **103** (2012) 1500.
55. H. Ahyayauch, M. Raab, J. V. Busto, N. Andraka, J. L. R. Arrondo, et al., Biophys. J. **103** (2012) 453.
56. R. P. Mason, J. D. Estermyer, J. F. Kelly, and P. E. Mason, Biochem. Bioph. Res. Co. **222** (1996) 78.
57. S. Dante, T. Hauss, R. Steitz, C. Canale, and N. A. Dencher, BBA-Biomembranes **1808** (2011) 2646.
58. H. Dies, L. Toppozini, and M. C. Rheinstädter, PLOS ONE DOI:101371/journalpone0099124 (2014).
59. K. Hristova and S. H. White, Biophys. J. **74** (1998) 2419.
60. A. M. D'Ursi, M. R. Armenante, R. Guerrini, S. Salvadori, G. Sorrentino, et al., J. Med. Chem. **47** (2004) 4231.
61. O. Crescenzi, S. Tomaselli, R. Guerrini, S. Salvadori, A. M. D'Ursi, et al., Eur. J. Biochem. **269** (2002) 5642.

62. A. Buchsteiner, T. Hauß, S. Dante, and N. Dencher, Biochim. Biophys. Acta **1798** (2010) 1969.
63. A. Buchsteiner, T. Hauß, and N. A. Dencher, Soft Matter **8** (2012) 424.
64. M. C. Rheinstädter, K. Schmalzl, K. Wood, and D. Strauch, Phys. Rev. Lett. **103** (2009) 128104.
65. I. Casuso, P. Sens, F. Rico, and S. Scheuring, Biophys. J. **99** (2010) L47.
66. H. W. Huang, Biochemistry **39** (2000) 8347.
67. D. M. Engelman, Y. Chen, C. N. Chin, A. R. Curran, A. M. Dixon, et al., FEBS Lett. **555** (2003) 122.
68. M. Heyden, J. A. Freites, M. B. Ulmschneider, S. H. White, and D. J. Tobias, Soft Matter **8** (2012) 7742.
69. R. Malathi and I. M. Johnson, J. Biomol. Struct. Dyn. **18** (2001) 709.
70. S. Rajamani, A. Vlassov, S. Benner, A. Coombs, F. Olasagasti, et al., Origins Life Evol. B. **38** (2008) 57.
71. J. Kraut and L. Jensen, Acta Crystallogr. **16** (1963) 79.
72. L. S. Bartell, L. S. Su, and H. Yow, Inorg. Chem. **9** (1970) 1903.
73. L. Toppozini, H. Dies, D. W. Deamer, and M. C. Rheinstädter, PLOS ONE **8** (2013) e62810.